

Quantum Hall states for Rydberg atoms with laser-assisted dipole-dipole interactions

Tian-Hua Yang,^{1, 2, *} Bao-Zong Wang,^{1, 2, *} Xin-Chi Zhou,^{1, 2} and Xiong-Jun Liu^{1, 2, 3, 4, †}

¹*International Center for Quantum Materials and School of Physics, Peking University, Beijing 100871, China*

²*Collaborative Innovation Center of Quantum Matter, Beijing 100871, China*

³*Institute for Quantum Science and Engineering and Department of Physics, Southern University of Science and Technology, Shenzhen 518055, China*

⁴*CAS Center for Excellence in Topological Quantum Computation, University of Chinese Academy of Sciences, Beijing 100190, China*

Rydberg atoms with dipole-dipole interactions provide intriguing platforms to explore exotic quantum many-body physics. Here we propose a novel scheme with laser-assisted dipole-dipole interactions to realize synthetic magnetic field for Rydberg atoms in a two-dimensional array configuration, which gives rise to the exotic bosonic topological states. In the presence of an external effective Zeeman splitting gradient, the dipole-dipole interaction between neighboring Rydberg atoms along the gradient direction is suppressed, but can be assisted when Raman lights are applied to compensate the energy difference. With this scheme we generate a controllable uniform magnetic field for the complex spin-exchange coupling model, which can be mapped to hard core bosons coupling to an external synthetic magnetic field. The highly tunable flat Chern bands of the hard core bosons are then obtained and moreover, the bosonic fractional quantum Hall states can be achieved with experimental feasibility. This work opens an avenue for the realization of the highly-sought-after bosonic topological orders using Rydberg atoms.

Introduction.—The two-dimensional (2D) electrons coupled to an external magnetic field in the perpendicular direction can fill into Landau levels, giving rise to the prominent quantum Hall (QH) effects [1, 2], whose discovery opened up the extensive search for topological states of quantum matter [3–7]. Unlike the electrons which are fermions, no quantum Hall states are obtained for noninteracting bosons coupled to external magnetic field, since the bosons are condensed to the ground state at zero temperature, rather than filling into an entire Landau band. To realize QH phase for bosons necessitates strong repulsive interactions, so that the Bose liquids become incompressible and the bosonic QH effects may be reached [8–14]. In comparison with fermionic counterparts, the bosonic integer and fractional QH states are all strongly correlated topological phases, being intrinsic [15, 16] or symmetry-protected topological orders [17–19]. Important attempts at achieving the QH regime have been made in bosonic systems like rotating Bose-Einstein condensates [20], Hostadter-Hubbard model [21], and interacting photons [22], while the feasibility of fully realizing such strongly correlated topological phases in experiment is hitherto elusive.

Recently, the exploration of novel correlated quantum states using Rydberg atoms attracted remarkable interests [23]. The Rydberg atoms can be arranged individually in array configuration through optical tweezers [24–26]. The highly excited internal states enable the long-range dipole-dipole interactions, which generate effective hopping couplings between Rydberg atoms at different sites [27, 28]. Such configuration simulates the hard-core bosons in lattice and provides versatile platforms to explore correlated bosonic quantum matter. Several important fundamental correlated phases have been observed in experiment, including quantum magnetism [29–

32], the 1D bosonic Su-Schrieffer-Heeger model [28], and 2D quantum spin liquid [33]. To further realize the bosonic QH phase with Rydberg arrays necessitates the generation of synthetic magnetic field which is associated with complex-valued dipole-dipole interactions. The synthetic gauge fields are key ingredient to explore topological physics, and have been actively studied for ultracold atoms in optical lattices [34–47]. Being intrinsically strongly correlated quantum simulators, the Rydberg arrays with synthetic magnetic fields are of great interests.

In this letter, we propose a novel mechanism dubbed *laser-assisted dipole-dipole interaction* for realizing a tunable synthetic magnetic field for hard-core bosons simulated by Rydberg atoms in a 2D array configuration. The realized model is described by the Hamiltonian

$$H = \sum_{j_x, j_y} (J_x b_{j_x+1, j_y}^\dagger b_{j_x, j_y} + J_y e^{i\Phi j_x} b_{j_x, j_y+1}^\dagger b_{j_x, j_y} + h.c.) \\ + \sum_{j_x, j_y} (J_{d_1} e^{i\Phi j_x} b_{j_x+1, j_y+1}^\dagger b_{j_x, j_y} + h.c.) \\ + \sum_{j_x, j_y} (J_{d_2} e^{i\Phi j_x} b_{j_x-1, j_y+1}^\dagger b_{j_x, j_y} + h.c.), \quad (1)$$

where $b_{i,j}^\dagger$ ($b_{i,j}$) creates (annihilates) a hard-core boson at site (i, j) with particle number $\langle b_{i,j}^\dagger b_{i,j} \rangle \leq 1$, the coefficients $J_{x(y)}$ and $J_{d_{1(2)}}$ characterize the nearest neighbor (NN) hopping term along x (y) direction and next-nearest neighbor (NNN) hopping terms in two diagonal directions, respectively. The hopping phase Φ represents a synthetic magnetic flux for the hard-core bosons, and is induced by the Raman laser-assisted dipole-dipole interactions. With the generated synthetic magnetic field, the flat Chern bands of the hard core bosons are obtained, with their flatness being drastically tuned by the diagonal

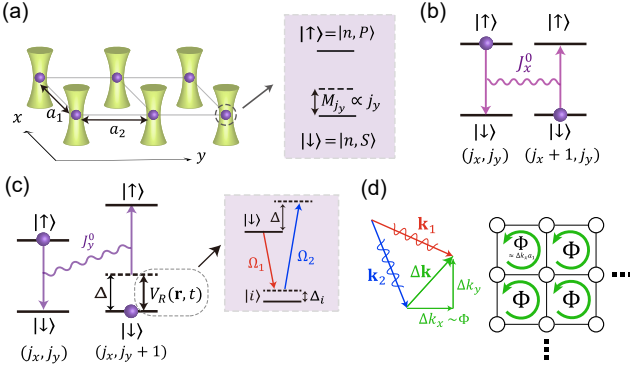


Figure 1. Sketch of the proposal. (a) Rydberg atoms trapped in optical tweezers to form a 2D array. An energy shift with gradient in y -direction modifies the energy difference between the two Rydberg states (effective Zeeman splitting for pseudospin). (b) Rydberg dipole-dipole interaction can induce spin exchange coupling between adjacent sites along the x -direction. (c) In y -direction, the spin exchange coupling is suppressed by the effective Zeeman energy offset. A two-photon Raman process compensates this energy offset and leads to the laser-assisted spin exchange couplings. (d) The laser-assisted exchange couplings have a spatially dependent phase, generating a synthetic magnetic flux in the 2D lattice.

J_{d_1, d_2} terms. This study may pave the way for realizing bosonic QH states with Rydberg arrays.

Laser-assisted dipole-dipole interactions.—We consider the 2D rectangular array of Rydberg atoms, with lattice constants $a_{1,2}$ and each trapped in optical tweezers [see Fig. 1(a)]. Two Rydberg states are chosen to simulate pseudo-spin-1/2 at each site, with $|\downarrow\rangle \equiv |n, S\rangle$ and $|\uparrow\rangle \equiv |n, P\rangle$. An effective Zeeman splitting M_{j_y} between the two pseudospin states is introduced, with $M_{j_y+1} - M_{j_y} = \Delta$ along the y -direction, while the on-site energy along x -direction is uniform. The total Hamiltonian of the system

$$H = H_{\text{dipole}} + H_{\text{Zeeman}} + V_R(\mathbf{r}, t) \quad (2)$$

includes the bare dipole-dipole interactions [23] which we take up to diagonal terms

$$\begin{aligned} H_{\text{dipole}} = & \sum_{j_x, j_y} (J_y^0 \sigma_{j_x, j_y}^+ \sigma_{j_x+1, j_y}^- + J_y^0 \sigma_{j_x, j_y}^+ \sigma_{j_x, j_y+1}^-) \\ & + \sum_{j_x, j_y} J_d^0 \sigma_{j_x, j_y}^+ \sigma_{j_x+1, j_y \pm 1}^- + h.c., \end{aligned}$$

the effective Zeeman energy gradient term

$$H_{\text{Zeeman}} = \frac{1}{2} \sum_{j_x, j_y} M_{j_y} \sigma_{j_x, j_y}^z,$$

and the Raman coupling potential

$$V_R(\mathbf{r}, t) = \frac{\Omega_1 \Omega_2^*}{\Delta_i} e^{i\Delta\mathbf{k} \cdot \mathbf{r}} e^{i(\omega_2 - \omega_1)t} \sigma_{j_x, j_y}^x + h.c..$$

In the above Hamiltonian, the dipole-dipole interaction leads to a spin exchange coupling J_x^0 between adjacent

sites along the x -direction, as illustrated in Fig. 1(b). The key ingredient of the scheme is that the bare exchange couplings J_y^0 and J_d^0 are suppressed by the relatively large Zeeman splitting offset Δ , but can be further induced by applying the Raman coupling potential V_R which is generated by two Raman lights with the Rabi-frequencies $\Omega_{1,2}$ and frequency difference $\omega_2 - \omega_1 \approx \Delta$ such that the Zeeman energy offset Δ is compensated by the two-photon process. Specifically, this Raman process is obtained by coupling one of the pseudospins to an intermediate state $|i\rangle$ with detuning Δ_i [see Fig. 1(c)]. With this configuration, the effective exchange couplings along the y and diagonal directions are recovered by the Raman laser-assisted dipole-dipole interactions. Furthermore, the the wave vector difference $\Delta\mathbf{k} = \mathbf{k}_1 - \mathbf{k}_2$ of two Raman lights determines the phases of the induced exchange couplings which are responsible to the magnetic flux in the effective model [Fig. 1(d)].

With the above analysis we can compute the effective exchange couplings through a time-dependent perturbation theory (see Supplemental Material for details [48])

$$\begin{aligned} J_y^{\text{eff}} = & J_y^0 \frac{\Omega_1 \Omega_2^*}{\Delta \Delta_i} e^{i(\Phi_{j_x} + \phi_{j_y})} (e^{i\phi_y} - 1), \\ J_{d_1(d_2)}^{\text{eff}} = & J_d^0 \frac{\Omega_1 \Omega_2^*}{\Delta \Delta_i} e^{i(\Phi_{j_x} + \phi_{j_y})} [e^{i(\phi_y + (-)\Phi)} - 1], \end{aligned} \quad (3)$$

where $\Phi = \Delta k_x a_1$ is a nontrivial phase generating flux in each plaquette, and the phase $\phi_y = \Delta k_y a_2$ tunes the strengths of J_y and $J_{d_1(d_2)}$. The term $e^{i\phi_y j_y}$ is however trivial and can be gauged out. We then reach the effective spin model in a more compact form

$$\begin{aligned} H_{\text{eff}} = & \sum_{j_x, j_y} (J_x \sigma_{j_x+1, j_y}^+ \sigma_{j_x, j_y}^- + J_y e^{i\Phi_{j_x}} \sigma_{j_x, j_y+1}^+ \sigma_{j_x, j_y}^- \\ & + h.c.) + \sum_{j_x, j_y} (J_{d_1} e^{i\Phi_{j_x}} \sigma_{j_x+1, j_y+1}^+ \sigma_{j_x, j_y}^- + h.c.) \\ & + \sum_{j_x, j_y} (J_{d_2} e^{i\Phi_{j_x}} \sigma_{j_x-1, j_y+1}^+ \sigma_{j_x, j_y}^- + h.c.), \end{aligned} \quad (4)$$

where J_y and $J_{d_1(d_2)}$ denote the amplitudes of the effective exchange couplings, and $J_x = J_x^0$. The above model is mapped to the Hamiltonian (1) for hard-core bosons by defining the bosonic operator $b_j^\dagger = |\uparrow\rangle_j \langle \downarrow|_j$ for the pseudo-spin-1/2 at each site.

We note that the Eq. (3) is obtained in the perturbative regime and holds precisely when Δ is large compared with the bare exchange couplings and the two-photon Raman coupling strength, namely $J_{y,d}^0/\Delta \ll 1$ and $|\Omega_1 \Omega_2^*|/(\Delta \Delta_i) \ll 1$. However, the generation of the magnetic flux through the laser-assisted dipole-dipole interactions is actually valid for more generic case beyond perturbative regime. The only difference is that for a moderate Δ , higher-order processes and additional intermediate processes will also contribute to the effective exchange couplings, which mainly quantitatively modify the amplitudes in Eq.(3), as we show below.

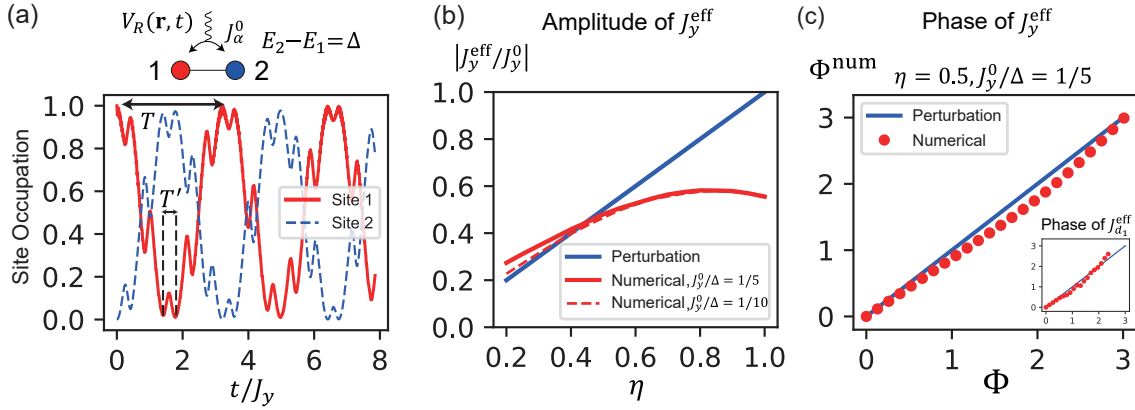


Figure 2. Numerical simulation for the laser-assisted exchange couplings and the synthetic magnetic flux under $\phi_y = \pi$. (a) Raman coupling driven Rabi-oscillation on a two-site system, which has an energy offset Δ compensated by the Raman potential. A boson is initialized at site 1 and evolves afterwards. Take $\eta = 2 |\Omega_1 \Omega_2 / (\Delta \Delta_i)| = 0.5$ and $\Delta = 5 J_y^0 = 10 J_y$. The slow-oscillation is driven by the Raman coupling, while the fast oscillations of frequency Δ correspond to the off-resonant bare transition. (b) The amplitude of J_y^{eff} matches well with the perturbative result $|J_y^{\text{eff}}| = \eta J_y^0$ when η and J_y^0/Δ are small. When η is large, $|J_y^{\text{eff}}|$ deviates clearly from the perturbation results. (c) The phase of the exchange couplings J_y , J_{d_1} and J_{d_2} (not shown in figure). The numerical results show good coincidence with perturbation results.

We confirm the above results numerically by studying the hopping dynamics for a single boson along the y direction or diagonal direction, as shown in Fig. 2. We initialize the state of single boson occupying the site 1, and numerically simulate the Rabi-oscillations by computing the dynamical evolution between the two sites from the original Hamiltonian (2), with which we determine the numerical result of J_y^{eff} (the numerical study for $J_{d_1(d_2)}^{\text{eff}}$ is similar, see Supplementary Material [48]). Fig. 2(a) shows an example of the Rabi-oscillations, from which one can read off directly the amplitude of the J_y^{eff} . From the phase accumulation in the wave function evolution, one can determine the phase φ of the exchange coupling coefficient. Further, to obtain the numerical result of the magnetic flux per plaquette, denoted as Φ^{num} , we compute $\varphi(j_x)$ in two separate simulations for the two-site system along y direction, respectively at $j_x = 0$ and $j_x = 1$. Then the flux is given by $\Phi^{\text{num}} = \varphi(j_x = 1) - \varphi(j_x = 0)$ [48]. Based on this procedure and with different parameters, in Fig. 2 (b,c) we numerically obtain Φ^{num} and J_y^{eff} (blue solid lines), and compare with the perturbation results in Eq. (3) (red dashed lines). We find that for relatively small J_y^0/Δ and $|\Omega_1 \Omega_2|/(\Delta \Delta_i)$, the numerical results of the amplitude of the laser-assisted exchange coupling $|J_y^{\text{eff}}|$ match better those given from the perturbation theory [Fig. 2(b)]. In comparison, the numerical results for the flux Φ^{num} matches well the perturbation results in more generic results [Fig. 2(c)]. With this we see that in the generic case the laser-assisted exchange couplings are induced, together with a nontrivial phase generating the magnetic flux in the effective model.

Before proceeding we provide estimates for the model parameters in the real experiment. For the ^{87}Rb atoms,

for instance, we may take the primary quantum number $n \sim 50$ for the Rydberg states, which are of the lifetime $\tau \sim 100\mu\text{s}$ at low temperature [49]. The lattice constants $a_{1,2}$ can be taken to be $10 \sim 20\mu\text{m}$, for which the bare exchange coupling is about $J_{x,y}^0 \approx 1 \sim 2\text{MHz}$. Accordingly, it is sufficient to set the effective Zeeman splitting offset as $\Delta \approx 5.0 \sim 10\text{MHz}$ to suppress the bare exchange couplings along the y and diagonal directions. When a Raman coupling with strength $\Omega_1 \Omega_2 / \Delta_i \sim 0.25$ is applied, the effective coupling of magnitudes $J_y \sim 0.6\text{MHz}$ to 1.0MHz is induced through numerical calculation.

As a key ingredient of the present scheme, the effective Zeeman splitting offset between neighboring sites can be realized with various approaches in the real experiment. For example, one can apply additional optical lights, which can be set together with the optical tweezer lights, to couple one of the two Rydberg states say $|\downarrow\rangle$ and the ground state $5S$ for ^{87}Rb atoms (or other low-energy normal states), giving an AC Stark shift to the Rydberg state $|\downarrow\rangle$. Using the same optical tweezer technique one can readily control the light field strength on each array at different j_y sites to realize the required effective Zeeman splitting offset. Another direct approach is apply a magnetic field with spatial gradient along y direction, which induces the real Zeeman energy splitting between the S and P Rydberg atoms. More details can be found in the Supplementary Material [48].

Flat Chern bands for Rydberg states.—We proceed to study the Chern band physics of the realized Hamiltonian (1), which exhibit novel features. In particular, in the presence of the NNN hopping $J_{d_{1(2)}}$, the energy spectra versus the flux $\Phi = (p/q)2\pi$ (with p and q being mutually prime integers) exhibits distinct characters

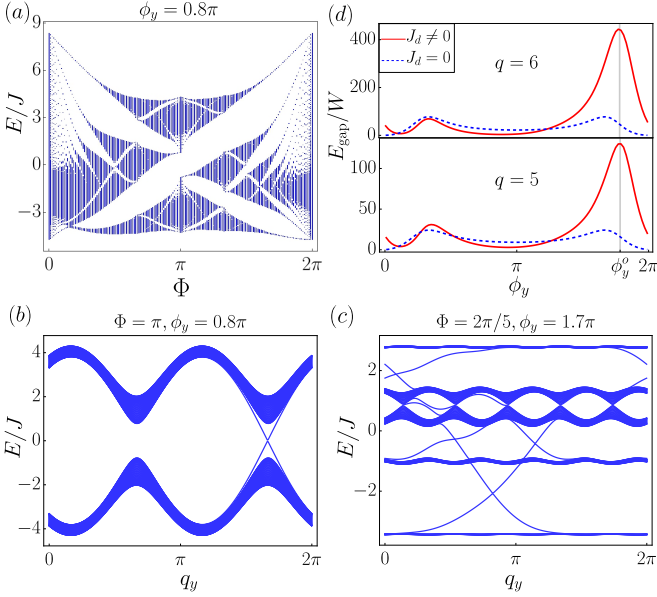


Figure 3. The deformed Hofstadter butterfly and Quantum Hall bands modulated by the diagonal hoppings $J_{d1}(d_2)$ when $J_x^0 = J_y^0$. (a) The deformed Hofstadter butterfly is generated at $\phi_y = 0.8\pi$. (b)-(c) The Chern bands for different ϕ_y and Φ . (d) The flatness ratio E_{gap}/W versus ϕ_y . The red solid lines show the flatness ratio for the realized model, in comparison with the case of setting $J_d = 0$ by hand (blue dashed line corresponding). The maximal flatness is obtained at $\phi_y = \phi_y^o$.

in comparison with the conventional Hofstadter butterfly which is symmetric with respect to both Φ and energy [50, 51]. Specifically, here the energy spectra are generically asymmetric, showing a deformed Hofstadter butterfly diagram [Fig. 3(a)]. Interestingly, for the π -flux regime, the bulk is gapped with nonzero Chern number [Fig. 3(b)], in contrast to the conventional case without diagonal terms, where the bulk is gapless [51]. For $q = 5$, a highly-flat lowest Chern band is obtained [Fig. 3(c)].

The intriguing feature is that the NNN hopping coefficients $J_{d1(2)}$ can drastically change the flatness ratio between the band gap E_{gap} and band width W regarding the lowest Chern band. Fig. 3(d) shows numerically the flatness ratio (the red solid lines) versus ϕ_y which governs J_y and $J_{d1(d_2)}$ via Eq. (3), and for comparison the flatness ratio for the case of setting $J_d = J_{d1,2} = 0$ by hand is also given (the blue dashed lines). We find that the flatness of the lowest band is greatly improved in a large range of ϕ_y . Especially, at $\phi_y = \phi_y^o \approx 1.7\pi$ for $J_x^0 = J_y^0$, the diagonal hoppings $J_{d1} = 0.1e^{i0.55\pi}$ and $J_{d2} = 0.6e^{i0.85\pi}$, for which the flatness ratio is optimized to maximum and is very large. This feature enables a feasible way to realize bosonic fractional QH states.

Bosonic 1/2 Laughlin state.—The flat Chern bands for hard-core bosons facilitate the realization of bosonic fractional QH states. In comparison with rotating Bose-Einstein condensates [14], the present Rydberg system

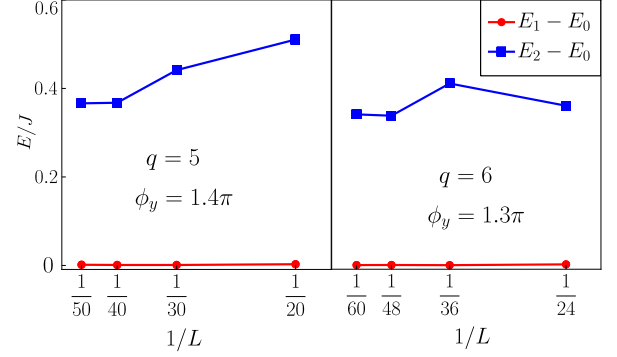


Figure 4. 1/2-fractional QH state shown from low energy spectra $E_n - E_0$ versus the system size $1/L$, with $L = L_x \times L_y$. The results show the two-fold degeneracy of the many-body ground states, which have a finite gap separating from the excited states. Other parameters are taken $J_x = J_y = J$.

realizes ideal Landau bands for hard-core bosons without necessitating fast-rotating condition. Also, unlike the Hofstadter model for ultracold atoms in optical lattice, the present model intrinsically reaches the strong interacting limit without suffering higher band effects. We denote the number of hard-core bosons as N_b , and the filling factor $\nu = N_b/N_\varphi$, where N_φ is the total magnetic flux threading the 2D array. As a prominent example, we consider the filling $\nu = 1/2$, the ground many-body wave function of this Bosonic Laughlin state reads [52]

$$\Psi_{gs}(z_1, \dots, z_{N_b}) = \prod_{j < k} (z_j - z_k)^2 \exp\left(-\sum_{i=1}^{N_b} |z_i|^2\right), \quad (5)$$

where $z_j = x_j + iy_j$ is the coordinate in the complex plane of the j th particle. The $\nu = 1/2$ fractional QH state is characterized by two fundamental features. First, the many-body ground states have two-fold degeneracy. Second, the ground state manifold is separated from excitations with a finite gap. Below we confirm the two features based on exact diagonalization for a finite system of $L_x \times L_y$ sites with periodic boundary condition.

The numerical results are shown in Fig. 4, where the hopping coefficients are set as $J_x = J_y = J$ for convenience at the phase $\phi_y = 1.4\pi$ (1.3π) for $q = 5$ (6). We compute the lowest three many-body eigenstates of the system, with energies $E_{0,1,2}$ and plot the spectra versus system size. We find the results are stabilized with sizes up to 5×10 for $q = 5$ and 6×10 for $q = 6$ with filling $\nu = 1/2$. We see clearly that there is two-fold degeneracy for the many-body ground states as $E_1 - E_0 \approx 0$, while the excitation gap $E_{\text{gap}} = E_2 - E_1$ approaches an appreciable magnitude at large-size limit. This yields the gap $E_{\text{gap}} = 0.37J$ for $q = 5$ and $E_{\text{gap}} = 0.35J$ for $q = 6$ for the present fractional QH phase.

Conclusions.—We have proposed a novel scheme dubbed *laser-assisted dipole-dipole interactions* for Rydberg atoms to realize synthetic magnetic field and 2D

bosonic QH states. The dipole-exchange interaction along one direction of the 2D Rydberg array is suppressed by setting an effective Zeeman splitting gradient, but can be assisted by applying a two-photon Raman coupling process which compensates the neighboring-site Zeeman energy offset and generates nontrivial gauge flux for the spin-exchange model. The tunable flat Chern bands of hard-core bosons and the bosonic fractional QH states can be obtained feasibly, with the 1/2-Laughlin state being illustrated. This work introduces a basic scheme of laser-assisted dipole-dipole interaction which can greatly expand the capability of engineering Rydberg atoms coupling to synthetic gauge fields and can be broadly applied to various Rydberg array configurations, hence may open an avenue to realize exotic correlated topological models and explore the highly-sought-after bosonic topological orders with experimental feasibility.

Acknowledgement.—We thank Shi Yu and Zheng-Xin Liu for fruitful discussions. This work was supported by National Key Research and Development Program of China (2021YFA1400900), the National Natural Science Foundation of China (Grants No.11825401, No.12104205), and the Strategic Priority Research Program of Chinese Academy of Science (Grant No. XDB28000000).

* These authors contribute equally to the work.

† Corresponding author: xiongjunliu@pku.edu.cn

- [1] K. V. Klitzing, G. Dorda, and M. Pepper, New method for high-accuracy determination of the fine-structure constant based on quantized Hall resistance, *Phys. Rev. Lett.* **45**, 494 (1980).
- [2] D. C. Tsui, H. L. Stormer, and A. C. Gossard, Two-dimensional magnetotransport in the extreme quantum limit, *Phys. Rev. Lett.* **48**, 1559 (1982).
- [3] M. Z. Hasan and C. L. Kane, Colloquium: Topological insulators, *Rev. Mod. Phys.* **82**, 3045 (2010).
- [4] X.-L. Qi and S.-C. Zhang, Topological insulators and superconductors, *Rev. Mod. Phys.* **83**, 1057 (2011).
- [5] B. Yan and S.-C. Zhang, Topological materials, *Rep. Prog. Phys.* **75**, 096501 (2012).
- [6] C.-K. Chiu, J. C. Y. Teo, A. P. Schnyder, and S. Ryu, Classification of topological quantum matter with symmetries, *Rev. Mod. Phys.* **88**, 035005 (2016).
- [7] B. Yan and C. Felser, Topological materials: Weyl semimetals, *Annu. Rev. Condens. Matter Phys.* **8**, 337 (2017).
- [8] N. K. Wilkin, J. M. F. Gunn, and R. A. Smith, Do attractive bosons condense? *Phys. Rev. Lett.* **80**, 2265 (1998).
- [9] N. K. Wilkin and J. M. F. Gunn, Condensation of "Composite Bosons" in a Rotating BEC, *Phys. Rev. Lett.* **84**, 6 (2000).
- [10] B. Paredes, P. Fedichev, J. I. Cirac, and P. Zoller, $\frac{1}{2}$ -Anyons in Small Atomic Bose-Einstein Condensates, *Phys. Rev. Lett.* **87**, 010402 (2001).
- [11] N. R. Cooper, N. K. Wilkin, and J. M. F. Gunn, Quantum phases of vortices in rotating Bose-Einstein condensates, *Phys. Rev. Lett.* **87**, 120405 (2001).
- [12] T. -L. Ho, Bose-Einstein Condensates with Large Number of Vortices, *Phys. Rev. Lett.* **87**, 060403 (2001).
- [13] A. S. Sørensen, E. Demler, and M. D. Lukin, Fractional quantum Hall states of atoms in optical lattices, *Phys. Rev. Lett.* **94**, 086803 (2005).
- [14] Alexander L. Fetter, Rotating trapped bose-einstein condensates, *Rev. Mod. Phys.* **81**, 647 (2009).
- [15] X.-G. Wen, Topological orders and edge excitations in fractional quantum Hall states, *Advances in Physics*, **44**, 405-473 (1995).
- [16] X. Chen, Z.-C. Gu, X.-G. Wen, Local unitary transformation, long-range quantum entanglement, wave function renormalization, and topological order, *Phys. Rev. B* **82**, 155138 (2010).
- [17] X. Chen, Z.-C. Gu, X.-G. Wen, Symmetry protected topological orders and the group cohomology of their symmetry group, *Phys. Rev. B* **87**, 155114 (2013).
- [18] Y.-M. Lu and A. Vishwanath, Theory and classification of interacting integer topological phases in two dimensions: A Chern-Simons approach, *Phys. Rev. B* **86**, 125119 (2012).
- [19] T. Senthil and M. Levin, Integer quantum hall effect for bosons, *Phys. Rev. Lett.* **110**, 046801 (2013).
- [20] N. Gemelke, E. Sarajlic, and S. Chu, Rotating few-body atomic systems in the fractional quantum Hall regime, *arXiv:1007.2677*.
- [21] M. E. Tai, A. Lukin, M. Rispoli, R. Schittko, T. Menke, D. Borgnia, P. M. Preiss, F. Grusdt, A. M. Kaufman, and M. Greiner, Microscopy of the interacting Harper Hofstadter model in the two-body limit, *Nature* **546**, 523 (2017).
- [22] L. W. Clark, N. Schine, C. Baum, N. Jia, and J. Simon, Observation of Laughlin states made of light, *Nature* **582**, 41 (2020).
- [23] A. Browaeys and T. Lahaye, Many-body physics with individually controlled Rydberg atoms, *Nat. Phys.* **16**, 132 (2020).
- [24] D. Barredo, S. de Léséleuc, V. Lienhard, T. Lahaye, and A. Browaeys, An atom-by-atom assembler of defect-free arbitrary two-dimensional atomic arrays, *Science* **354**, 1021 (2016).
- [25] M. Endres, H. Bernien, A. Keesling, H. Levine, E. R. Anschuetz, A. Krajenbrink, C. Senko, V. Vuletic, M. Greiner, and M. D. Lukin, Atom-by-atom assembly of defect-free one-dimensional cold atom arrays, *Science* **354**, 1024 (2016).
- [26] D. Barredo, V. Lienhard, S. de Léséleuc, T. Lahaye, and A. Browaeys, Synthetic three-dimensional atomic structures assembled atom by atom, *Nature* **561**, 79 (2018).
- [27] S. de Léséleuc, V. Lienhard, P. Scholl, D. Barredo, S. Weber, N. Lang, H. P. Büchler, T. Lahaye, and A. Browaeys, Observation of a symmetry-protected topological phase of interacting bosons with Rydberg atoms, *Science* **365**, 775 (2019).
- [28] S. K. Kanungo, J. D. Whalen, Y. Lu, M. Yuan, S. Dasgupta, F. B. Dunning, K. R. A. Hazzard, and T. C. Killian, Realizing topological edge states with Rydberg-atom synthetic dimensions, *Nat. Com.* **13**, 972 (2022).
- [29] H. Labuhn, D. Barredo, S. Ravets, S. Léséleuc, T. Macrì, T. Lahaye, and A. Browaeys, Tunable two-dimensional arrays of single Rydberg atoms for realizing quantum Ising models, *Nature* **534**, 667 (2016).
- [30] H. Bernien, S. Schwartz, A. Keesling, H. Levine, A. Om-

ran, H. Pichler, S. Choi, A. S. Zibrov, M. Endres, M. Greiner, V. Vuletić, and M. D. Lukin, Probing many-body dynamics on a 51-atom quantum simulator, *Nature* **551**, 579 (2017).

[31] P. Scholl, M. Schuler, H. J. Williams, A. A. Eberharter, D. Barredo, K.-N. Schymik, V. Lienhard, L.-P. Henry, T. C. Lang, T. Lahaye, A. M. Läuchli, and A. Browaeys, Quantum simulation of 2D antiferromagnets with hundreds of Rydberg atoms *Nature* **595**, 233 (2021).

[32] S. Ebadi, T. T. Wang, H. Levine, A. Keesling, G. Semeghini, A. Omran, D. Bluvstein, R. Samajdar, H. Pichler, W. W. Ho, S. Choi, S. Sachdev, M. Greiner, V. Vuletić, and M. D. Lukin, Quantum phases of matter on a 256-atom programmable quantum simulator, *Nature* **595**, 227 (2021).

[33] G. Semeghini, H. Levine, A. Keesling, S. Ebadi, T. T. Wang, D. Bluvstein, R. Verresen, H. Pichler, M. Kalinowski, R. Samajdar, A. Omran, S. Sachdev, A. Vishwanath, M. Greiner, V. Vuletić, and M. D. Lukin, Probing topological spin liquids on a programmable quantum simulator, *Science* **374**, 1242 (2021).

[34] D. Jaksch and P. Zoller, Creation of effective magnetic fields in optical lattices: the Hofstadter butterfly for cold neutral atoms, *New J. Phys.* **5**, 56 (2003).

[35] J. Struck, C. Ölschläger, M. Weinberg, P. Hauke, J. Simonet, A. Eckardt, M. Lewenstein, K. Sengstock, and P. Windpassinger, Tunable gauge potential for neutral and spinless particles in driven optical lattices, *Phys. Rev. Lett.* **108**, 225304 (2012).

[36] M. Aidelsburger, M. Atala, M. Lohse, J. T. Barreiro, B. Paredes, and I. Bloch, Realization of the Hofstadter Hamiltonian with ultracold atoms in optical lattices, *Phys. Rev. Lett.* **111**, 185301 (2013).

[37] H. Miyake, G. A. Siviloglou, C. J. Kennedy, W. C. Burton, and W. Ketterle, Realizing the Harper Hamiltonian with laser-assisted tunneling in optical lattices, *Phys. Rev. Lett.* **111**, 185302 (2013).

[38] M. Aidelsburger, M. Lohse, C. Schweizer, M. Atala, J. Barreiro, S. Nascimbène, N. Cooper, I. Bloch, and N. Goldman, Measuring the Chern number of Hofstadter bands with ultracold bosonic atoms, *Nat. Phys.* **11**, 162 (2015).

[39] X. -J. Liu, Z. -X. Liu, K. T. Law, V. W. Liu, and T. K. Ng, Chiral topological orders in an optical Raman lattice, *New J. Phys.* **18**, 035004 (2016).

[40] B. K. Stuhl, H.-I. Lu, L. M. Aycock, D. Genkina, and I. B. Spielman, Visualizing edge states with an atomic Bose gas in the quantum Hall regime, *Science* **349**, 1514 (2015).

[41] G. Jotzu, M. Messer, R. Desbuquois, M. Lebrat, T. Uehlinger, D. Greif, and T. Esslinger, Experimental realization of the topological Haldane model with ultracold fermions, *Nature* **515**, 237 (2014).

[42] N. Goldman and J. Dalibard, Periodically driven quantum systems: effective Hamiltonians and engineered gauge fields, *Phys. Rev. X* **4**, 031027 (2014).

[43] X.-J. Liu, K. Law, and T. Ng, Realization of 2D Spin-Orbit Interaction and Exotic Topological Orders in Cold Atoms, *Phys. Rev. Lett.* **112**, 086401 (2014).

[44] Z. Wu, L. Zhang, W. Sun, X.-T. Xu, B.-Z. Wang, S.-C. Ji, Y. Deng, S. Chen, X.-J. Liu, and J.-W. Pan, Realization of two-dimensional spin-orbit coupling for Bose-Einstein condensates *Science* **354**, 83 (2016).

[45] B. Song, L. Zhang, C. He, T. F. J. Poon, E. Ha-jiyev, S. Zhang, X.-J. Liu, and G.-B. Jo, Observation of symmetry-protected topological band with ultracold fermions, *Sci. Adv.* **4**, eaao4748 (2018).

[46] Y.-H. Lu, B.-Z. Wang, and X.-J. Liu, Ideal Weyl semimetal with 3D spin-orbit coupled ultracold quantum gas, *Sci. Bull.* **65**, 2080 (2020).

[47] Z.-Y. Wang, X.-C. Cheng, B.-Z. Wang, J.-Y. Zhang, Y.-H. Lu, C.-R. Yi, S. Niu, Y. Deng, X.-J. Liu, S. Chen, and J.-W. Pan, Realization of an ideal Weyl semimetal band in a quantum gas with 3D spin-orbit coupling, *Science* **372**, 271 (2021).

[48] See Supplemental Material for details of the (i) Time-dependent Perturbation Theory, (ii) Experimental Parameters and (iii) Numerical simulation of two-site dynamics, which includes Ref. [49, S1, S2, S3, S4, S5, S6, S7, S9, S10, S11, S12, S13]

[49] I. I. Beterov, I. I. Ryabtsev, D. B. Tretyakov, and V. M. Entin, Quasiclassical calculations of blackbody-radiation-induced depopulation rates and effective lifetimes of Rydberg nS , nP , and nD alkali-metal atoms with $n \leq 80$, *Phys. Rev. A* **79**, 052504 (2009).

[50] P. G. Harper, Single Band Motion of Conduction Electrons in a Uniform Magnetic Field, *Proc. Phys. Soc. London Sect. A* **68**, 874 (1955).

[51] D. R. Hofstadter, Energy levels and wave functions of Bloch electrons in rational and irrational magnetic fields, *Phys. Rev. B* **14**, 2239 (1976).

[52] V. Kalmeyer and R. B. Laughlin, Equivalence of the resonating-valence-bond and fractional quantum Hall states, *Phys. Rev. Lett.* **59**, 2095 (1987).

[53] D. Barredo, H. Labuhn, S. Ravets, T. Lahaye, A. Browaeys, and C. S. Adams, Coherent excitation transfer in a spin chain of three Rydberg atoms, *Phys. Rev. Lett.* **114**, 113002 (2015).

[54] C. S. Adams, J. D. Pritchard, and J. P. Shaffer, Assembled arrays of Rydberg-interacting atoms, *Journal of Physics B: Atomic, Molecular and Optical Physics* **53**, 012002 (2020).

[55] L. Béguin, A. Vernier, R. Chicireanu, T. Lahaye, and A. Browaeys, Direct measurement of the van der Waals interaction between two Rydberg atoms, *Phys. Rev. Lett.* **110**, 263201 (2013).

[56] T. F. Gallagher, *Rydberg atoms*, Cambridge monographs on atomic, molecular, and chemical physics No. 3 (Cambridge University Press, Cambridge ; New York, 1994)

[57] A. Ramos, R. Cardman, and G. Raithel, Measurement of the hyperfine coupling constant for $nS_{1/2}$ Rydberg states of ^{85}Rb , *Phys. Rev. A* **100**, 062515 (2019).

[58] R. Löw, H. Weimer, J. Nipper, J. B. Balewski, B. Butscher, H. P. Büchler, and T. Pfau, An experimental and theoretical guide to strongly interacting Rydberg gases, *Journal of Physics B: Atomic, Molecular and Optical Physics* **45**, 113001 (2012).

[59] J. Lampen, H. Nguyen, L. Li, P. R. Berman, and A. Kuzmich, Long-lived coherence between ground and Rydberg levels in a magic-wavelength lattice, *Phys. Rev. A* **98**, 033411 (2018).

[60] E. Gomez, S. Aubin, L. A. Orozco, and G. D. Sprouse, Lifetime and hyperfine splitting measurements on the 7s and 6p levels in rubidium, *Journal of the Optical Society of America B* **21**, 2058 (2004).

[61] R. F. Gutterres, C. Amiot, A. Fioretti, C. Gabbanini, M. Mazzoni, and O. Dulieu, Determination of the ^{87}Rb 5p

state dipole matrix element and radiative lifetime from the photoassociation spectroscopy of the $\text{Rb}_2 0_g^-(P_{3/2})$ long-range state, Phys. Rev. A **66**, 024502 (2002).

[62] R. Song, J. Bai, Y. Jiao, J. Zhao, and S. Jia, Lifetime Measurement of Cesium Atoms Using a Cold Rydberg

Gas, Appl. Sci. **12**, 2713 (2022).

[63] D. J. Griffiths and D. F. Schroeter, *Introduction to quantum mechanics, third edition ed.* (Cambridge University Press, Cambridge ; New York, NY, 2018).

[64] D. Steck, *Rubidium 87 D Line Data*, (2003) .

Supplementary Material: Quantum Hall states for Rydberg atoms with laser-assisted dipole-dipole interactions

S-1. TIME-DEPENDENT PERTURBATION THEORY

In this section, we derive the effective exchange couplings J_y^{eff} and $J_{d_1(d_2)}^{\text{eff}}$ using the time-dependent perturbation theory. Start with the Hamiltonian $H = H_{\text{dipole}} + H_{\text{Zeeman}} + V_R(\mathbf{r}, t)$, with H_{dipole} and H_{Zeeman} given in main text. The Raman process, which consists of two Raman lasers coupling $|\downarrow\rangle$ to a low-lying intermediate state $|i\rangle$, can be described as

$$V_R(\mathbf{r}, t) = \sum_j [(\Omega_1 e^{i\mathbf{k}_1 \cdot \mathbf{r}} e^{-i\omega_1 t} + \Omega_2 e^{i\mathbf{k}_2 \cdot \mathbf{r}} e^{-i\omega_2 t}) |\downarrow\rangle_{j_x, j_y} \langle i|_{j_x, j_y} + h.c.] + (\Delta_i - \omega_1) |i\rangle_{j_x, j_y} \langle i|_{j_x, j_y}. \quad (\text{S1})$$

Consider the assisted hopping J_y^{eff} between two adjacent sites $j = (j_x, j_y)$ and $j' = (j_x, j_y + 1)$. We denote $|a\rangle = |j = \uparrow, j' = \downarrow\rangle$ and $|b\rangle = |j = \downarrow, j' = \uparrow\rangle$. The exchange couplings between $|a\rangle$ and $|b\rangle$ are suppressed by the large Zeeman splitting offset Δ , and are further recovered by applying the Raman coupling potential V_R : a two-photon process compensating the energy offset can take place either on the site j or j' , as shown in the Fig. S1. In the first case, the compensation is essentially obtained by the Raman coupling between spin down state $|\downarrow\rangle_j$ and intermediate state $|i\rangle_j$. Therefore, all information about this channel is contained in the three-dimensional subspace spanned by $|a\rangle, |b\rangle$ and $|c\rangle = |j = i, j' = \uparrow\rangle$. Similarly, the compensation on site j' happens in the subspace spanned by $|a\rangle, |b\rangle$ and $|c'\rangle = |j = \uparrow, j' = i\rangle$. Therefore, we may calculate the assisted hopping amplitude in such three-level subspaces.

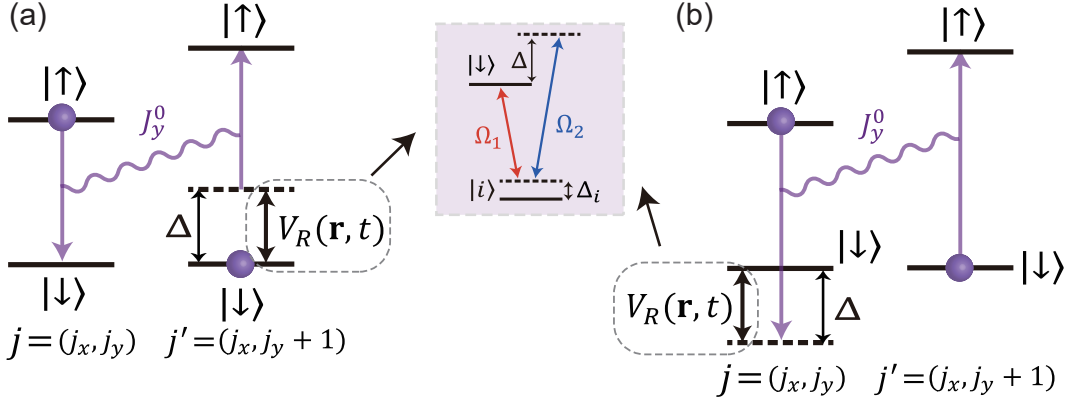


Figure S1. The possible laser-assisted transition processes between two sites. In both cases, a two-photon process between $|\downarrow\rangle$ and $|i\rangle$ on one site compensates an energy difference Δ . The intermediate state can be (a) $|j = \downarrow, j' = i\rangle$ or (b) $|j = i, j' = \downarrow\rangle$. The two processes add up to give the total effective transition moment.

Consider the channel where compensation happens at site j' . The effective Hamiltonian under the basis $(|a\rangle, |c'\rangle, |b\rangle)$ can be written as

$$H_{\text{TL}} = \begin{pmatrix} E_a & \Omega_1 e^{i\mathbf{k}_1 \cdot \mathbf{r}'} e^{-i\omega_1 t} + \Omega_2 e^{i\mathbf{k}_2 \cdot \mathbf{r}'} e^{-i\omega_2 t} & J_y^0 \\ \Omega_1^* e^{-i\mathbf{k}_1 \cdot \mathbf{r}'} e^{i\omega_1 t} + \Omega_2^* e^{-i\mathbf{k}_2 \cdot \mathbf{r}'} e^{i\omega_2 t} & E_{c'} & E_b \\ J_y^0 & & E_b \end{pmatrix}. \quad (\text{S2})$$

The diagonal terms are the energies for the three states, respectively, satisfying $E_b - E_a = \Delta$ and $E_{c'} - E_a = \Delta - \omega_1$.

Quantity	Typical Value	Quantity	Typical Value
Rydberg principal quantum number n	50	Rydberg state lifetime	around $100\mu\text{s}$
Lattice spacing (in x -direction) a_1	$15\mu\text{m}$	Raman laser wavelength	1000nm
Rydberg atomic radius [S6]	$0.16\mu\text{m}$	Detuning of Raman processes Δ_i	25GHz
Dipole-dipole interaction strength J	1MHz	Energy difference between 5S and 5P	around 90THz
Detuning Δ	10MHz	$\Omega_{1,2}$	250MHz
Fine structure of Rydberh states	around 1GHz	Transition dipole moment $\langle 50, S e \mathbf{r} 6, P \rangle$	$0.01ea_0$
Hyperfine splitting of Rydberg states	less than 200kHz	Raman laser field strength	$3 \times 10^5 \text{ V/m}$
Spacing between n and $n + 1$ Rydberg states	60GHz	The minimal Raman laser angle	5°

Table I. Estimates of values for the relevant physical quantities.

For simplicity of notation, we denote $\Omega_l(\mathbf{r}) = \Omega_l e^{i\mathbf{k}_l \cdot \mathbf{r}}$ for $l = 1, 2$. Transferring to interaction picture gives

$$H_{\text{TL}}^{(i)} = \begin{pmatrix} 0 & \Omega_1(j') e^{i(-\omega_1 - E_{c'} + E_a)t} + \Omega_2(j') e^{i(-\omega_2 - E_{c'} + E_a)t} & J_y^0 e^{-i\Delta t} \\ \Omega_1(j')^* e^{-i(-\omega_1 - E_{c'} + E_a)t} + \Omega_2(j')^* e^{-i(-\omega_2 - E_{c'} + E_a)t} & 0 & 0 \\ J_y^0 e^{i\Delta t} & 0 & 0 \end{pmatrix}. \quad (\text{S3})$$

Employing time-dependent perturbation theory, we consider possible channels for the transition $|b\rangle\langle a|$ in the Dyson series. The first-order process is the bare transition, which is off-resonant. There are no second-order processes for this transitions. Two third-order processes exist, manifesting themselves in the Dyson series as

$$U^{(3)}(t) = -i^3 \int_0^t dt_1 \int_0^{t_1} dt_2 \int_0^{t_2} dt_3 H_{31}(t_1) H_{12}(t_2) H_{21}(t_3) + H_{31}(t_1) H_{13}(t_2) H_{31}(t_3).$$

Recursive integration yields multiple terms, but most are off-resonant and suppressed. Notably, a term in the first integrand reads

$$U_{\text{Raman}}^{(3)} = \frac{\Omega_1(j') \Omega_2(j')^* J_y^0 (e^{-i(\Delta + \omega_2 - \omega_1)t} - 1)}{(-\omega_1 - E_{c'} + E_a)(\omega_2 - \omega_1)(\Delta + \omega_2 - \omega_1)}. \quad (\text{S4})$$

This is an equivalent Rabi transition of amplitude $\frac{\Omega_1(j') \Omega_2(j')^* J_y^0}{\Delta_i \Delta}$ and detuning $\Delta - (\omega_1 - \omega_2)$, which is resonant when $\omega_1 - \omega_2 = \Delta$. A similar derivation goes when we choose $|c\rangle$ as the intermediate state. Combining these two channels, we have a resonant transition amplitude

$$J_y^{\text{eff}} = \frac{\Omega_1 \Omega_2^*}{\Delta \Delta_i} e^{i(\Delta k_x a_1 j_x + \Delta k_y a_2 j_y)} (e^{i\Delta k_y a_2} - 1) J_y^0. \quad (\text{S5})$$

Similarly one can derive the expression for $J_{d_1(d_2)}^{\text{eff}}$. This leads to Eq. (3) of the main text.

Processes of other order in the perturbation series may lead to deviations from the above result. Some higher-order processes may affect the effective hopping, because a resonance can also be recovered by multiple compensations. Each two-photon process corrects J_y by multiplying a factor $\eta = \frac{2|\Omega_1 \Omega_2|}{|\Delta_i \Delta|}$ (a factor 2 appears here because each compensation process can happen on either of the two sites), so resonant $2n$ -photon processes have an amplitude of around $\eta^n J_y^0$. When η is finite such that higher powers of η cannot be ignored, these processes will also contribute to J_y^{eff} . This at most modifies the amplitude of J_y^{eff} but not its phase, however, since the condition of resonance makes additional phase factors cancel. On the other hand, when J_y^0/Δ is finite, the off-resonant bare transition (zeroth-order) is not fully suppressed. Naively, this increases the amplitude of the transition and dilute the phase, since the zeroth-order process has no phase. However, the effect of this bare transition may not manifest itself as a simple modification of J_y^{eff} , since a resonant process and an off-resonant one cannot be added straightforwardly. In experiments, the exact phase and amplitude of J_y^{eff} may be determined through a calibration process by sweeping the parametric space.

S-2. EXPERIMENTAL PARAMETERS

In this section, we give the estimate of the orders of magnitude of the relevant experimental parameters. To be specific, the data given here are based on ^{87}Rb atoms. We choose Rydberg states $|\downarrow\rangle = |50, S\rangle$ and $|\uparrow\rangle = |50, P\rangle$

as the pseudospin. A dipole-dipole interaction of strength $J_{ij} = \frac{C_3}{r_{ij}^3}$ exists between such two states, where $C_3 \approx 3400 \text{MHz} \cdot \mu\text{m}^3$ [S1, S2]. On a rectangular lattice with lattice constants $a_{1,2}$, we have

$$J_x^0 = \frac{C_3}{a_1^3}, \quad J_y^0 = \frac{C_3}{a_2^3}, \quad (S6)$$

and

$$J_{d_1}^0 = J_{d_2}^0 = \frac{C_3}{(a_1^2 + a_2^2)^{3/2}}. \quad (S7)$$

Since J_y^{eff} has an amplitude smaller than J_y^0 , we may choose a_2 slightly smaller than a_1 to make $J_y^{\text{eff}} = J_x^0$. For example, with $\phi_y = \pi$ and $\frac{\Omega_1 \Omega_2}{\Delta \Delta_i} = \frac{1}{4}$, we can choose $a_1 = 15 \mu\text{m}$ and $a_2 = 2^{-\frac{1}{3}} a_1 \approx 12 \mu\text{m}$, so that $J_x^0 = J_y^{\text{eff}} = J = 1 \text{MHz}$. In this case $J_{d_1}^{\text{eff}} = J_{d_2}^{\text{eff}} = 0.24 \text{MHz}$ when $\Phi = 0$. The next resonant term is the next nearest neighbor hopping in x -direction, with an amplitude $J_{x(2)}^0 = J_x^0/2^3 = 0.125 \text{MHz}$, which we ignore. Van der Waals interaction can also be ignored, as it is well less than 100kHz in this case [S3]. Given the interaction strength, the effective Zeeman energy gradient Δ can be chosen as 10MHz, giving a ratio $\frac{J_y^0}{\Delta} = \frac{1}{5}$.

We have to ensure that no other undesired states or processes mix into our Hamiltonian. The two pseudospin states are separated by an energy of about 20GHz. The fine structure splittings of $n = 50$ Rydberg states are about hundreds of MHz [S4, Chap. 16] and the hyperfine structure splittings are at the level of 200kHz [S5]. We can see that the effective Zeeman splitting is much larger than the hyperfine energy and small enough compared to fine structure splittings. The intermediate state $|i\rangle$ is chosen as one of the 6P states. The Raman lasers would only couple $|\downarrow\rangle$ to this intermediate state, but not $|\uparrow\rangle$, because a single-photon process reverses parity and the $|50, P\rangle(|\uparrow\rangle) \rightarrow |6, P\rangle$ transition is forbidden. Another process $|50, P\rangle(|\uparrow\rangle) \rightarrow |6, S\rangle$ is possible from the point of view of parity, but is suppressed by an energy detuning of about 90THz. Other possible processes are detuned even more. Thus, as long as one chooses $\Delta_i < 100 \text{GHz}$, other processes are at least three orders of magnitude smaller.

The strengths of the Raman lasers are labeled as $\Omega_{1,2}$, which equals to the electric field strength of the laser times the transition dipole moment. We can estimate that the transition dipole moment $\langle 50, S | e \mathbf{r} | 6, P \rangle \approx 0.01 e a_0$, where a_0 is the Bohr radius [S6]. This means that $\Omega_{1,2}(\text{Hz}) = 803 E_{1,2}(\text{V/m})$, with $E_{1,2}$ being the electric field strength. Thus experimental lasers can reach levels where $\Omega_{1,2} \sim$ hundreds of MHz. An exemplary data would be $\Delta_i = 25 \text{GHz}$ and $\Omega = 250 \text{MHz}$. The Raman lasers would have an approximate wavelength of $\lambda = 1000 \text{nm}$ as they couple 50S to 6P [S7]. The flux $\Phi = \Delta k_x a_1$ and the phase $\phi_y = \Delta k_y a_1$ generated by Raman coupling are expected to be on the order of π . Given the lattice constants chosen above, $|\mathbf{k}| \approx \frac{1}{20} \left| \frac{2\pi}{\lambda} \right|$ so the two lasers should have an intersecting angle of around 5° . To make the flux be accurate at or over 0.1π level, one would require tuning the laser angles at 0.5° level or better, which is well achievable in experiment.

To observe the correlated effects, the lifetime of the system should be large compared with characteristic time defined by the inverse of the system's energy scale. For $J = 1 \text{MHz}$, a lifetime of around $100 \mu\text{s}$ is desirable. A Rydberg state of principal quantum number $n \approx 50$ can indeed have a lifetime of over $100 \mu\text{s}$ at low temperatures [S8]. By coupling a Rydberg state to a 6P state, decay from the 6P state will also affect the lifetime. The lifetime of such processes should be much larger than that of the Rydberg state. The 6P states on their own have a lifetime of around 100ns [S9]. Under a detuned coupling, the wave function on that state would be $\frac{2\Omega_{1,2}}{\Delta_i}$, so the lifetime will be prolonged by a factor $(2\Omega_{1,2}/\Delta_i)^{-2}$. Choosing $\frac{\Omega_{1,2}}{\Delta_i} < \frac{1}{100}$ would be sufficient to ensure a lifetime much larger than $100 \mu\text{s}$.

For the creation of the effective Zeeman splitting using AC Stark effect, we can introduce an additional two-photon effective Raman coupling together with each optical tweezer, coupling the pseudospin state $|\downarrow\rangle = |50, S\rangle$ to the ground state $|5, S\rangle$. With a similar parity argument, $|\uparrow\rangle$ will not be coupled. This produces an energy shift $\Omega_{\text{Stark}}^2/\Delta_{\text{Stark}}$. With $\Omega_{\text{Stark}} = 200 \text{MHz}$ and $\Delta_{\text{Stark}} = 1 \text{GHz}$, a detuning of several tens of MHz can be achieved. By letting Ω_{Stark} vary from 0 to 200MHz along y direction, it is sufficient to realize the required effective Zeeman splitting gradient. The table I shows typical parameter conditions.

S-3. NUMERICAL SIMULATION OF TWO-SITE DYNAMICS

Suppose there are two sites with a resonant transition $J_\alpha e^{i\varphi}$ between them, where J_α is a real number represents the strength of transition. The Hamiltonian in two-dimensional subspace reads $H_2 = J_\alpha (\cos \varphi \sigma_x + \sin \varphi \sigma_y)$. Then

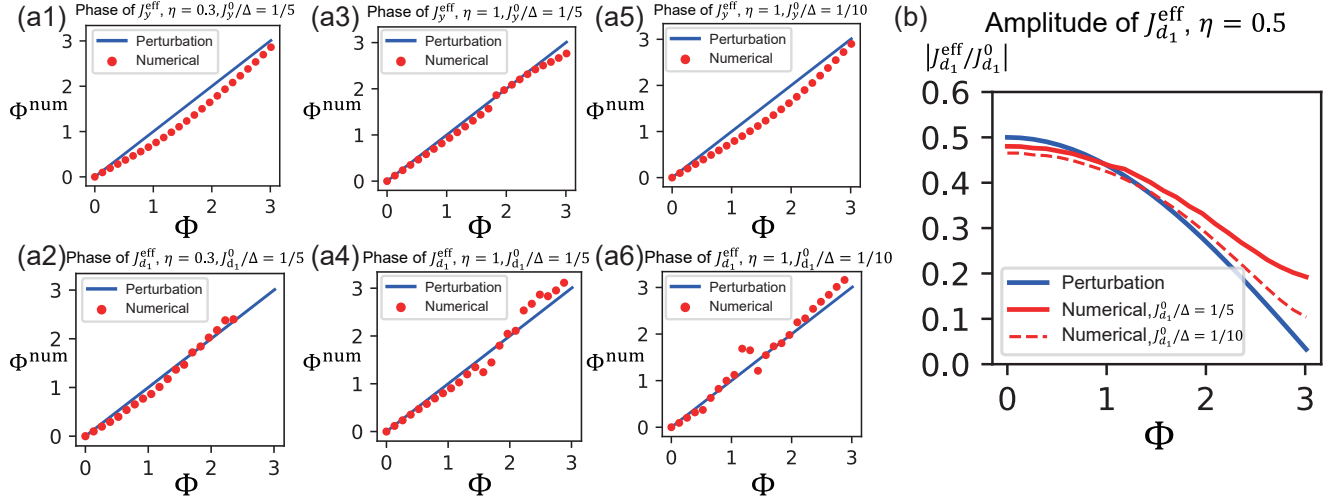


Figure S2. (a1-a6) The site-dependent phase of J_y^{eff} and $J_{d_1}^{\text{eff}}$ are plotted versus the applied Φ of the Raman potential under several sets of parameters, and with $\phi_y = \pi$. Aside from small numerical errors, the result matches the expectation that $J_{\alpha}^{\text{eff}} \propto e^{i\Phi j_x}$ for $\alpha = y, d_1$. This shows that the generated flux is robust under a wide range of $\eta = \left| \frac{2\Omega_1\Omega_2}{\Delta\Delta_i} \right|$ and J_y^0/Δ , even in regions where the amplitude of the effective transition deviates significantly from the perturbative result. (b) The amplitude of J_{d_1} roughly matches the perturbative formula $|J_{d_1}^{\text{eff}}| = \eta J_{d_1}^0 \sin\left(\frac{\phi_y + \Phi}{2}\right)$. The match is better at small $J_{d_1}^0/\Delta$. Both results for J_{d_1} also hold for J_{d_2} .

the time evolution operator would be

$$e^{-iH_2t} = \begin{pmatrix} \cos(J_{\alpha}t) & ie^{-i\varphi} \sin(J_{\alpha}t) \\ -ie^{i\varphi} \sin(J_{\alpha}t) & \cos(J_{\alpha}t) \end{pmatrix}. \quad (\text{S8})$$

When a particle is initially placed at the site 1, the particle wave function would evolve with the time as

$$|\psi(t)\rangle \propto (\cos(J_{\alpha}t), -ie^{i\varphi} \sin(J_{\alpha}t))^T. \quad (\text{S9})$$

Therefore, the phase difference between two sites is obtained as $\varphi - \frac{\pi}{2}$ and J_{α} can be read off from the oscillation frequency of time evolution.

We take the simulation on the two sites with an energy difference Δ and Raman compensations on both sites. The Hamiltonian reads

$$\begin{aligned} H_{2s} = & \Delta|2\rangle\langle 2| + J_{\alpha}^0(|2\rangle\langle 1| + |1\rangle\langle 2|) \\ & + (\Omega_1(j_1)e^{-i\omega_1 t} + \Omega_2(j_1)e^{-i\omega_2 t})(|i\rangle\langle 1| + |1\rangle\langle i|) \\ & + (\Omega_1(j_2)e^{-i\omega_1 t} + \Omega_2(j_2)e^{-i\omega_2 t})(|i\rangle\langle 2| + |2\rangle\langle i|), \end{aligned} \quad (\text{S10})$$

where $|i\rangle$ is the intermediate state of Raman coupling, $j_1 = (j_x, j_y)$ and $j_2 = (j_x + \delta j_x, j_y + \delta j_y)$ are two adjacent sites. From the main text we know that the effective hopping is

$$J_{\alpha}^{\text{eff}} = \frac{\Omega_1\Omega_2}{\Delta\Delta_i} J_{\alpha}^0 \left(e^{i(\Phi\delta j_x + \phi_y\delta j_y)} - 1 \right) e^{i(\Phi j_x + \phi_y j_y)}. \quad (\text{S11})$$

Therefore, we have

$$J_{\alpha} = 2 \frac{\Omega_1\Omega_2}{\Delta\Delta_i} \sin\left(\frac{\Phi\delta j_x + \phi_y\delta j_y}{2}\right) J_{\alpha}^0, \quad (\text{S12})$$

$$\varphi = \Phi j_x + \phi_y j_y + \frac{\Phi\delta j_x + \phi_y\delta j_y + \pi}{2}. \quad (\text{S13})$$

Note that the flux $\Phi = \varphi(j_x + 1, j_y) - \varphi(j_x, j_y)$. We perform the real-time numerical simulations for the dynamical evolutions from the two-site Hamiltonian and fit the parameters to confirm the amplitudes and phases of J_y, J_{d_1}

and J_{d_2} . In the simulation of J_y , we set for convenience that $\delta j_x = 0$ and $\delta j_y = 1$, and $j_x = j_y = 0$ in light of the translational symmetry. Then we take the same numerical simulation at $j_x = 1$ and $j_y = 0$, and take the difference of φ measured in the two either cases to confirm the induced flux and that $J_y \propto e^{i\Phi j_x}$. The absolute value of the phase φ , which is not important, may be complicate and influenced by multiple factors, however the phase difference (flux) is fairly stable (main text). Similar simulation for J_{d_1} and J_{d_2} have been performed by taking $\delta j_x = \pm 1$ and $\delta j_y = \pm 1$ [see Fig. S2].

* These authors contribute equally to the work.

† Corresponding author: xiongjunliu@pku.edu.cn

- [S1] D. Barredo, H. Labuhn, S. Ravets, T. Lahaye, A. Browaeys, and C. S. Adams, Coherent excitation transfer in a spin chain of three Rydberg atoms, *Phys. Rev. Lett.* **114**, 113002 (2015).
- [S2] C. S. Adams, J. D. Pritchard, and J. P. Shaffer, Assembled arrays of Rydberg-interacting atoms, *Journal of Physics B: Atomic, Molecular and Optical Physics* **53**, 012002 (2020).
- [S3] L. Béguin, A. Vernier, R. Chicireanu, T. Lahaye, and A. Browaeys, Direct measurement of the van der Waals interaction between two Rydberg atoms, *Phys. Rev. Lett.* **110**, 263201 (2013).
- [S4] T. F. Gallagher, *Rydberg atoms*, Cambridge monographs on atomic, molecular, and chemical physics No. 3 (Cambridge University Press, Cambridge ; New York, 1994)
- [S5] A. Ramos, R. Cardman, and G. Raithel, Measurement of the hyperfine coupling constant for $nS_{1/2}$ Rydberg states of ^{85}Rb , *Phys. Rev. A* **100**, 062515 (2019).
- [S6] R. Löw, H. Weimer, J. Nipper, J. B. Balewski, B. Butscher, H. P. Büchler, and T. Pfau, An experimental and theoretical guide to strongly interacting Rydberg gases, *Journal of Physics B: Atomic, Molecular and Optical Physics* **45**, 113001 (2012)
- [S7] J. Lampen, H. Nguyen, L. Li, P. R. Berman, and A. Kuzmich, Long-lived coherence between ground and Rydberg levels in a magic-wavelength lattice, *Phys. Rev. A* **98**, 033411 (2018).
- [S8] I. I. Beterov, I. I. Ryabtsev, D. B. Tretyakov, and V. M. Entin, Quasiclassical calculations of blackbody-radiation-induced depopulation rates and effective lifetimes of Rydberg nS , nP , and nD alkali-metal atoms with $n \leq 80$, *Phys. Rev. A* **79**, 052504 (2009).
- [S9] E. Gomez, S. Aubin, L. A. Orozco, and G. D. Sprouse, Lifetime and hyperfine splitting measurements on the 7s and 6p levels in rubidium, *Journal of the Optical Society of America B* **21**, 2058 (2004).
- [S10] R. F. Gutterres, C. Amiot, A. Fioretti, C. Gabbanini, M. Mazzoni, and O. Dulieu, Determination of the ^{87}Rb 5p state dipole matrix element and radiative lifetime from the photoassociation spectroscopy of the $\text{Rb}_2 0_g^- (P_{3/2})$ long-range state, *Phys. Rev. A* **66**, 024502 (2002).
- [S11] R. Song, J. Bai, Y. Jiao, J. Zhao, and S. Jia, Lifetime Measurement of Cesium Atoms Using a Cold Rydberg Gas, *Appl. Sci.* **12**, 2713 (2022).
- [S12] D. J. Griffiths and D. F. Schroeter, *Introduction to quantum mechanics, third edition* ed. (Cambridge University Press, Cambridge ; New York, NY, 2018).
- [S13] D. Steck, *Rubidium 87 D Line Data*, (2003) .